PROCEEDINGS OF SCIENCE

Qualification of the first pre-production 3D FBK sensors with ITkPixV1 readout chip

G.Calderini,[a] **F.Crescioli,**[a] **G.-F.Dalla Betta,**[b,c] **G.Gariano,**[d] **C.Gemme,**[d] **F.Guescini,**[e] **S.Hadzic,**[e] **T.Heim,**[f] **A.Lapertosa,**[d,g,i] **S.Ravera,**[d,g] **M.Ressegotti,**[d,*] **A.Rummler,**[h] **Md.A.A.Samy,**[b,c] **D M S Sultan**[b,c] **and L.Vannoli**[d,g]

[a] *Centre National de la Recherche Scientifique, Paris, France*
[b] *Department of Industrial Engineering, University of Trento, Trento, Italy*
[c] *TIFPA INFN, Trento, Italy*
[d] *INFN Genoa, Genoa, Italy*
[e] *Max-Planck-Institut für Physik, Munich, Germany*
[f] *Lawrence Berkeley National Laboratory and University of California, Berkeley, USA*
[g] *Department of Physics, University of Genoa, Genoa, Italy*
[h] *European Laboratory for Particle Physics, CERN*
[i] *now at INFN Catania, Catania, Italy*

E-mail: martina.ressegotti@cern.ch

The ITk detector, the new ATLAS silicon tracking system for the High Luminosity LHC (HL-LHC), will be equipped with 3D pixel sensor modules in the innermost layer (L0). The pixel cell dimensions will be 25×100 μm^2 in the barrel and 50×50 μm^2 in the end-caps, with one readout electrode at the centre of each pixel and four bias electrodes at the corners. Sensors from pre-production wafers (50×50 μm^2) produced by FBK have been bump-bonded to ITkPixV1.1 chips at IZM. Bare modules have been assembled in Genoa on Single Chip Cards (SCCs) and characterized in laboratory measurements and in test beam campaigns. Some of these modules have been irradiated in Bonn and at the CERN IRRAD facility. Preliminary results of their characterization after irradiation are shown, including measurements performed during test beam campaigns at CERN SPS in Summer 2022.

12-16 December 2022
Santa Fe, New Mexico, USA

*Speaker

ATL-ITK-PROC-2023-005
31 January 2023

1. Introduction

After 2026, the Large Hadron Collider (LHC) will be upgraded to reach an instantaneous luminosity up to $7.5 \cdot 10^{34}$ cm^{-2}s^{-1} [1]. The ATLAS detector [2] will be upgraded as well, to cope with the increased pile-up and radiation damage. In particular, the tracking system will be replaced by a new all-silicon detector, the Inner Tracker (ITk, Figure 1), that will be installed during the Long Shutdown 3 (2026-2028), comprising a Pixel detector [4] in the innermost part surrounded by a large area Strip detector [5].

The Inner System consists of the two innermost layers of the ITk Pixel detector, L0 and L1. It is planned to be completely replaced after an integrated luminosity of 2000 fb^{-1} delivered by the HL-LHC. In the Pixel innermost layer (L0), the B0 layer in the barrel will be located at minimum 34 mm from the beam axis while the R0 and R0.5 rings in the end-caps will have a minimum distance of 33.2 mm from the beam axis. The modules are expected to be exposed to a non-ionising fluence of up to $1.7 \cdot 10^{16}$ n$_{eq}$/cm^2 (after 2000 fb^{-1}, including safety factors) and an ionising dose of up to 1 Grad. After several years of R&D [9], the 3D sensor technology was chosen due to its inherent radiation hardness. 3D sensors will be used in the L0 layers in the form of triplet modules (three front-ends bump-bonded onto three sensor dies). The modules will have 25×100 μm^2 pixel cells in the barrel region and 50×50 μm^2 pixel cells in the end-cap region. Their production is distributed among three manufacturing sites: CNM (sensors with 25×100 μm^2 pixel cells), FBK (50×50 μm^2 and 25×100 μm^2 pixel cells) and SINTEF (50×50 μm^2 pixel cells).

This paper reports on the characterization of the first pre-production 3D sensors with a pixel size of 50×50 μm^2 produced by FBK, bump-bonded to ITkPixV1.1 readout chips. They have been tested in the laboratory and in test beam campaigns at CERN PS [6] and SPS [7]. Measurements were conducted before and after irradiation with protons at the irradiation facilities in Bonn and IRRAD at CERN. The total irradiation resulted in a non-uniform fluence distribution with a peak value of $1.9 \cdot 10^{16}$ n$_{eq}$/cm^2 (average $1.5 \cdot 10^{16}$ n$_{eq}$/cm^2).

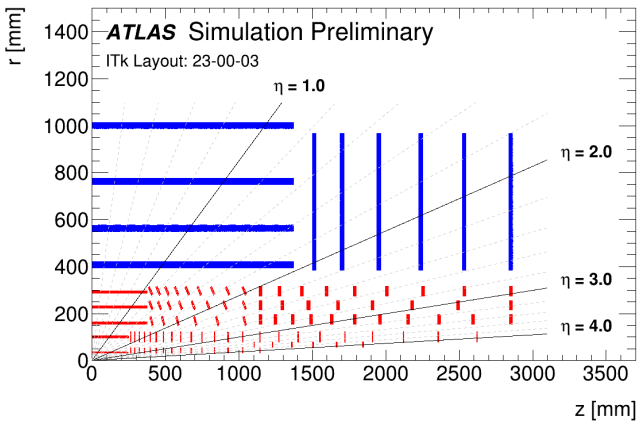

Figure 1: Schematic depiction of the ITk detector, including the Pixel (red) and Strip (blue) detectors [3].

2. Description of the samples under test

Sensors presented in this paper have been designed at the University of Trento and produced by FBK (Trento, Italy). The structure of the 3D pixel sensors and pixel cells is illustrated in Figure 2. More details are available in [8].

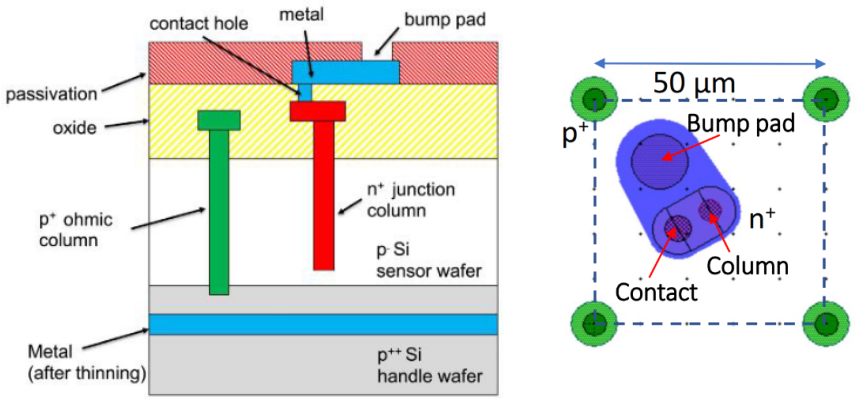

Figure 2: Schematic cross-section view of a 3D pixel sensor (left) built with single-sided technology (a p-spray layer to isolate the n^+ columns at the surface is not shown in the figure). Top view of the layout of a 3D pixel cell (right).

The ITkPix chip [10] is the ATLAS version of the RD53B chip designed by the RD53 Collaboration [11] for the ATLAS and CMS experiments with the goal to satisfy the stronger requirements on efficient and fast detection of signals as well as radiation hardness. It is designed in 65 nm feature size CMOS technology, where each sensor has an area of ~2×2 cm^2 and is composed of 384×400 pixels per chip (50×50 μm^2 pixel size). It is designed to operate at low thresholds (1000 electrons standard threshold), handle high data rates (4 data links per chip at 1.28 Gb/s), has a power dissipation of about 0.5 W/cm^2 and can withstand total ionising doses up to 1 Grad [12]. The latest available version of the ITkPix chip family is version ITkPixV1.1 which was used to build the modules whose results are shown in this publication. Some functions such as the Time Over Threshold (ToT) measurement are not available yet in this prototype. The version ITkPixV2 is about to be finalized and is targeted to be the version used in the final ITk Pixel detector.

Samples presented in this report are obtained by pre-production wafers delivered by FBK to CERN in 2021, out of which 20 sensors were diced and flip-chipped to ITkPixV1.1 chips at IZM. Six of the bare modules were delivered to Genoa where they were mounted on Single Chip Cards (SCCs, Figure 3), which are rigid PCBs for testing, resulting in the single-chip modules used for the first qualification.

3. Characterization of unirradiated samples

3.1 Characterization in laboratory

First tests were carried out in the laboratory with X-rays (Amptek Mini-X2 X-ray tube with Ag anode with tip located about 15 cm above the module). Data was collected with random trigger scans with 60 s duration. Most pixels detected ~6700 hits/pixel (~110 Hz), while a small fraction

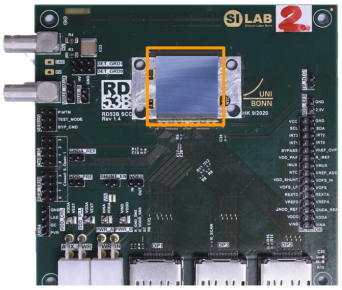

Figure 3: Module (orange rectangle) mounted on an SCC (front).

detected ~10000 hits/pixel (~170 Hz), as shown in Figure 4 left. In addition 18 pixels (0.01%) detected zero hits, of which 2 pixels were masked and the remaining 16 pixels are identified as pixels with disconnected bumps. Pixels with a higher number of detected hits than average tend to be located close to the edges of the sensor. This behaviour, also reported for planar sensors, for example in [14], can be explained by the electric field extending beyond the pixel cell into the slim edge region which then contributes to the charge collection (Figure 4 right).

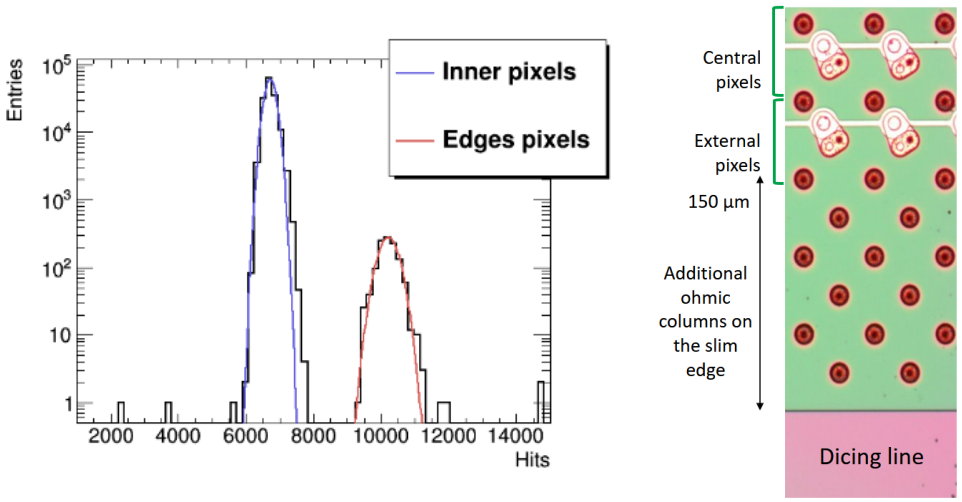

Figure 4: Distribution of pixel hit occupancy during a 60 s long scan with X-rays (left) [13]. External and central pixel cells, with additional ohmic columns outside the read out area (right).

3.2 Test beam setup and data analysis

Next, the performance of unirradiated samples was studied in test beam campaigns. The same setup [15] was used for all test beam campaigns mentioned in this report. It includes a telescope (ACONITE at SPS, AZAELA at PS) with six MIMOSA26 planes and a FE-I4 single chip module as a timing reference plane, two scintillators at the two ends of the setup whose coincidence triggers the signal readout via a Trigger Logic Unit (TLU) [16, 17], and a data acquisition system based on YARR [18] and EUDAQ [19]. The resulting position resolution delivered by the beam telescope on the surface of the Devices Under Test (DUTs) is ~2 µm [20].

Test beam data were analysed with the C++ based framework Corryvreckan [21], more details can be found in [22]. In particular, reconstructed particle tracks passing through disabled or masked

pixels on DUTs or through neighbouring pixels are not used in the efficiency calculation. Hence the resulting efficiency applies to pixels not masked or disabled.

3.3 Test beam results of unirradiated samples

Unirradiated modules were tested with beam at CERN PS (12 GeV hadron beam) and SPS (~120 GeV pion beam). The measured efficiency is >97.5% already with 0 V bias applied, as visible in Figure 5 left. This result is compatible with previous efficiency measurements [9] performed at DESY (~5 GeV electron beam) on similar sensors (50×50 μm^2 pixel cell prototype by FBK) bump-bonded to a RD53A chip [24].

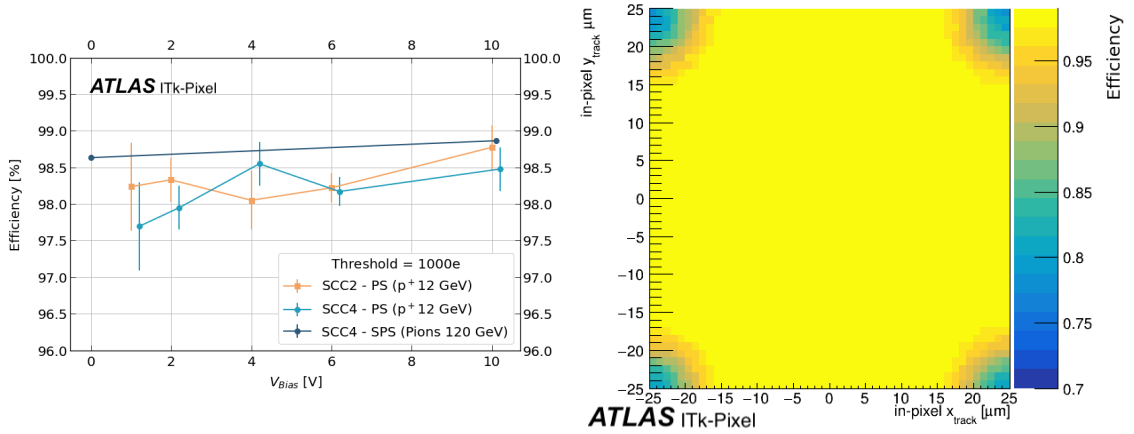

Figure 5: Efficiency of unirradiated modules as a function of reverse bias voltage, measured at CERN PS and SPS (left) and in-pixel efficiency measured at CERN SPS at 10 V reverse bias with module perpendicular to the beam direction (right). The threshold is tuned to 1000*e*. [23]. Efficiency values and their uncertainty in the left plot are respectively the mean and standard deviation of values measured in several runs of data taking with the same bias voltage applied and the same chip tuning.

Figure 5 right shows the hit efficiency as a function of the particle impact point over the surface of a pixel cell (*in-pixel* efficiency). The in-pixel efficiency was measured at SPS with the sensor fully depleted (10 V reverse bias voltage applied) and mounted perpendicular to the beam direction. As expected, lower efficiency zones are visible in the pixel cell corners corresponding to the p^+ columns, with an efficiency drop down to ~75% within a radius of about ~10 µm (the p^+ columns radius is about ~4 µm) from the pixel cell corners. The efficiency drop is expected to disappear if the sensor is tilted with respect to the beam direction, as it is shown in Figure 9 for an irradiated module. In the central part of the pixel cell the measured efficiency is higher than 99% and no structure (polySilicon cap or n^+ column, illustrated in Figure 2) is visible at the considered bias voltage. This behaviour may be explained by the fact that the p^+ columns pass through the entire thickness of the active layer, while the n^+ columns extend up to ~20 µm from the edge of the active layer (Figure 2 left). Thus charge can be generated below the n^+ coulmns.

4. Multiple irradiations

Two samples were irradiated sequentially at two different facilities: first in Bonn (May-June 2022) with a 14 MeV proton beam up to a fluence of $1 \cdot 10^{16}$ n_{eq}/cm^2 uniform across the sensor

surface, then at CERN IRRAD facility (September 2022) with a 24 GeV proton beam achieving a total non-uniform irradiation with an average fluence of $1.5 \cdot 10^{16}$ n_{eq}/cm^2 and a peak fluence of $1.9 \cdot 10^{16}$ n_{eq}/cm^2. During the first irradiation the modules were cooled at a temperature ranging from about -18°C to -50°C, while the second irradiation was performed without cooling. The details of irradiation campaigns are summarized in Table 1. During the second irradiation, devices were positioned inclined with respect to the beam (Figure 6 left) in order to increase the sensor's irradiated area and scanning horizontally during the irradiation, hence the spatial distribution of the fluence integrated at IRRAD is approximately uniform along the horizontal direction and gaussian along the vertical direction (following the beam profile). During the irradiation an aluminium dosimeter of approximately the same size of the sensor was placed on its back. After the irradiation it was cut in smaller pieces, the activity of the Na-22 peak of each piece was measured with a Ge detector and finally the fluence received by each Al piece was calculated from the activity measurement. This set of measurements was used to reconstruct the map of the sensor local fluence received during the second irradiation (Figure 6 right), that was used to study the measured efficiency as a function of fluence presented in section 5.2.2. The irradiated samples were tested in test beams at CERN SPS after each irradiation.

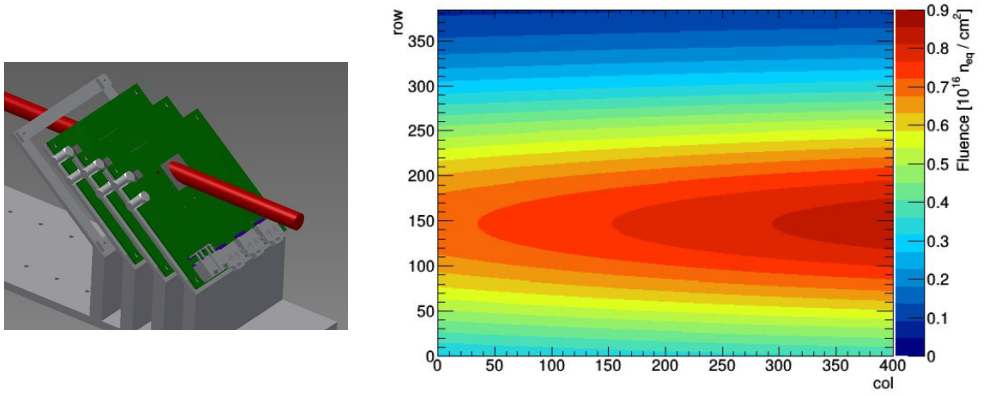

Figure 6: Schematic of the samples under irradiation at the IRRAD facility (left), with tilted SCCs (green), incident proton beam (red) and support structures (grey). Reconstruction of the fluence over a sensor (SCC3) received at the IRRAD facility, based on the Al foil measurements (right).

Facility	Beam	Type	Fluence [n_{eq}/cm^2]
Bonn	14 MeV protons	uniform	$1.0 \cdot 10^{16}$
IRRAD	24 GeV protons	non-uniform	$0.5 \cdot 10^{16}$ average
			$0.9 \cdot 10^{16}$ peak
Total		non-uniform	$1.5 \cdot 10^{16}$ average
			$1.9 \cdot 10^{16}$ peak

Table 1: Summary of irradiation campaigns performed on samples.

5. Characterization of irradiated samples

5.1 Tuning strategy and stability

The same tuning was used to collect all data during each test beam campaign for simplicity. The tuning was performed at 100 V reverse bias with a target threshold of 1000*e* and used for all bias voltage values applied to the sensors. Only the masking was updated as needed before/during data taking. As shown in Figure 7, threshold and noise distributions were reasonably stable over a large bias voltage range under these conditions. The tuning was performed at about -16°C and about -30°C for data collected after the first and the second irradiation, respectively.

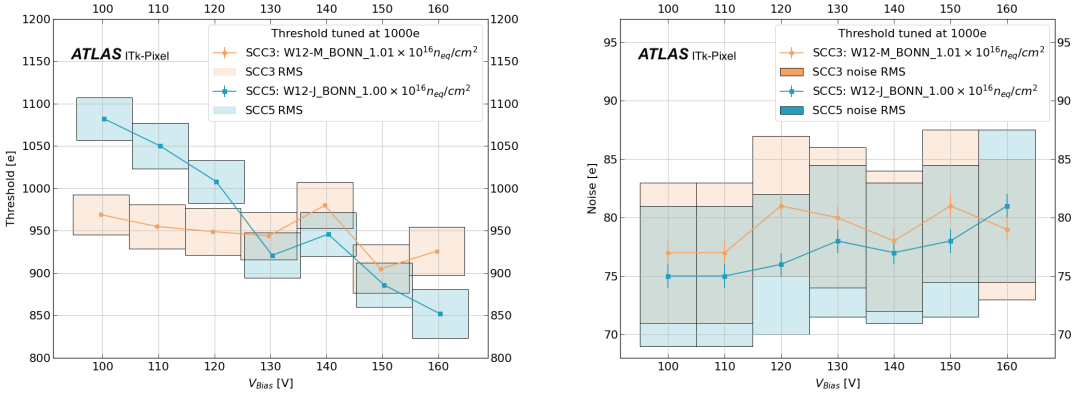

Figure 7: Threshold (left) and noise (right) distributions as a function of reverse bias voltage [23]. Error bars are the mean error of the threshold or noise distributions, columns are the standard deviation of the distribution. Data was taken after the first irradiation, similar results are obtained after the second irradiation.

5.2 Test beam results of irradiated samples

5.2.1 Hit efficiency as a function of bias voltage

Hit efficiency measurements of irradiated samples were performed at CERN SPS. Results as a function of the bias voltage after each irradiation are summarized in Figure 8. The module temperature during data taking ranged from about -30°C to -40°C. As the sensor area hit by the beam is smaller than the area of the sensor itself, for measurements performed at the highest received fluence ("ϕ up to 1.9" [$\cdot 10^{16}$ n_{eq}/cm^2] in Figure 8 legend) the samples were positioned so that the test beam hit the sensors approximately in the region that received the highest fluence. Hence, in such an area the average fluence is higher than the average fluence over the entire sensor's surface reported above, namely $\sim 1.7 \cdot 10^{16}$ n_{eq}/cm^2 and $\sim 1.6 \cdot 10^{16}$ n_{eq}/cm^2 (total fluence after two irradiation campaigns) for SCC3 and SCC5 respectively (peak value $1.9 \cdot 10^{16}$ n_{eq}/cm^2) and the hit efficiency measurements reported must be referred to such average values.

The graphs in Figure 8 middle and bottom show that the hit efficiency exceeds 97% at 40 V and at 100 V reverse bias voltage for fluence values of $1 \cdot 10^{16}$ n_{eq}/cm^2 (uniform) and $1.9 \cdot 10^{16}$ n_{eq}/cm^2 (peak) respectively when the incident track is perpendicular to the module. In addition, the graph in Figure 8 top demonstrates the expected behaviour that the hit efficiency increases if the beam

hits the sensor surface with an angle of 15°. The tilted configuration is more representative of the real conditions of sensors inside the ATLAS ITk detector, in which particle tracks will typically be inclined with respect to the sensors surface. The saturation values of the hit efficiency are ~98.5% for the perpendicular configuration and ~99.9% for the tilted configuration. This effect can be understood looking at the in-pixel efficiency: Figure 9 left confirms the presence of efficiency drops in the four pixel corners with perpendicular beam, observed also with unirradiated modules. Figure 9 right shows that such drops disappear when the sensor surface is not perpendicular to the beam and thus particles impinging next to the pixel cell corners are not passing all the way through the p^+ columns. This results in an overall increased hit efficiency in the tilted configuration.

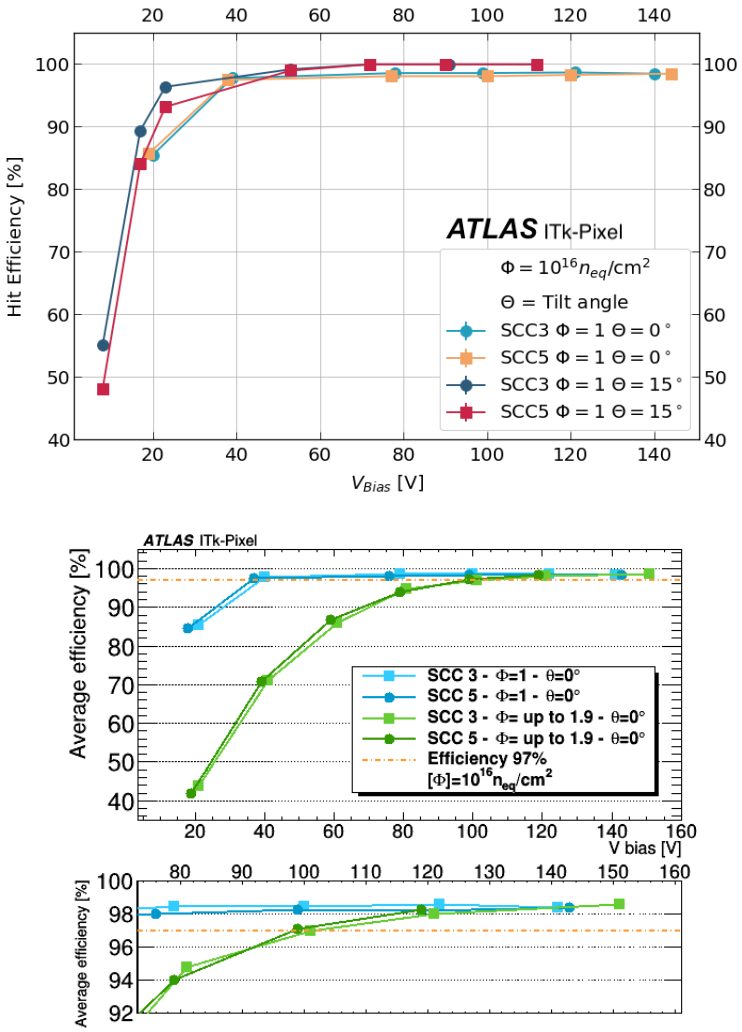

Figure 8: Efficiency as a function of reverse bias voltage after the first irradiation ($1 \cdot 10^{16}$ n_{eq}/cm^2 uniform) with sensor surface perpendicular and tilted by 15° with respect to the incident beam (top) [23]. Efficiency as a function of reverse bias voltage after both irradiation campaigns measured with sensor surface perpendicular to the incident beam (middle), and same curve zoomed in the region of the efficiency saturation values (bottom) [25].

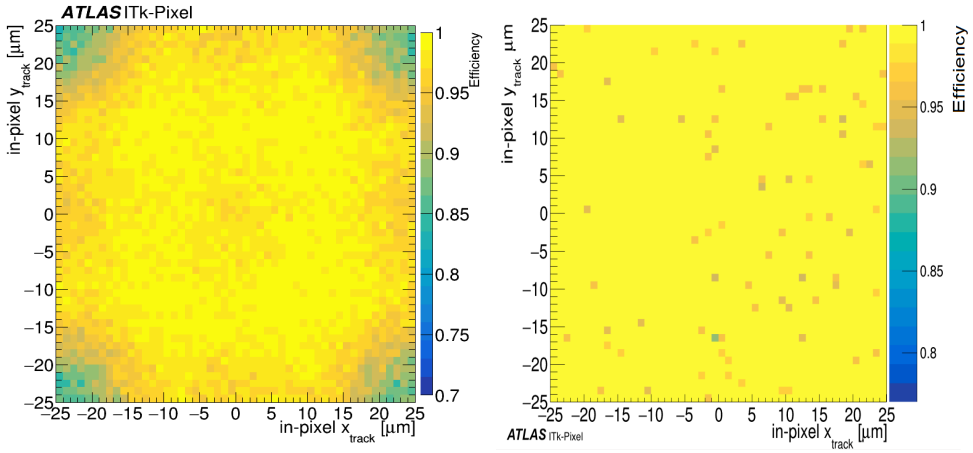

Figure 9: In-pixel efficiency measured with module perpendicular (left) [25] and tilted by 15° (right) [23] with respect to the beam direction with sensor fully depleted (100 V and 90 V reverse bias voltage applied respectively). The measurements are performed on modules that received the ultimate fluence up to $1.9 \cdot 10^{16}$ n_{eq}/cm^2 ($\sim 1.6 \cdot 10^{16}$ n_{eq}/cm^2 average in the beam region) for the perpendicular configuration (left) and a total fluence of $1 \cdot 10^{16}$ n_{eq}/cm^2 for the tilted configuration (right).

5.2.2 Hit efficiency as a function of fluence

The non-uniform irradiation dose integrated by the samples allowed to study their performance as a function of fluence using a limited number of modules. Three concentric regions on the modules' surface were defined, with a total received average fluence of $1.59 \cdot 10^{16}$ n_{eq}/cm^2, $1.70 \cdot 10^{16}$ n_{eq}/cm^2 and $1.78 \cdot 10^{16}$ n_{eq}/cm^2, respectively (defined in the legend of Figure 10 bottom) and used to compute the efficiency in different fluence ranges. As expected, a lower efficiency is achieved at the same bias voltage with increasing fluence (Figure 10 top). In particular, 97% efficiency is reached at ~80 V, ~100 V and ~110 V for the three fluence ranges, respectively (Figure 10 bottom).

5.2.3 Operability window

In order to evaluate the operability window of devices irradiated at the ultimate fluence value, the measured average efficiency and the characteristic IV curve are compared in Figure 7 left. First, when the average efficiency is as high as ~97% (100 V reverse bias) the leakage current is of the order of ~150 $\mu A/cm^2$ (scaled at −25 °C), corresponding to a power dissipation of 15 mW/cm^2. It can be concluded that the module can be operated in a reverse bias voltage range as wide as ~100 V to ~170 V requiring both high efficiency and operating below the breakdown voltage.

On the other hand, during the test beam campaigns an increase of noisy and disabled pixels was observed with increasing reverse bias voltage at the highest values applied. In order to qualitatively estimate this behaviour and show that pixels start to become noisy as the bias voltage increases, analog scans [26] were systematically performed as a function of the applied voltage (Figure 11 right). As the result strongly depends on the chip tuning, one should remember that the same tuning was used for the entire set of measurements as explained in section 5.1 and different results may be obtained with a different tuning strategy. Figure 11 right shows that the fraction of pixels failing the analog scan initially slowly increases (around a value of about ~3% failing pixels) up to about ~ 160 V, and has a faster rise next to the breakdown voltage. Thus an operability window between

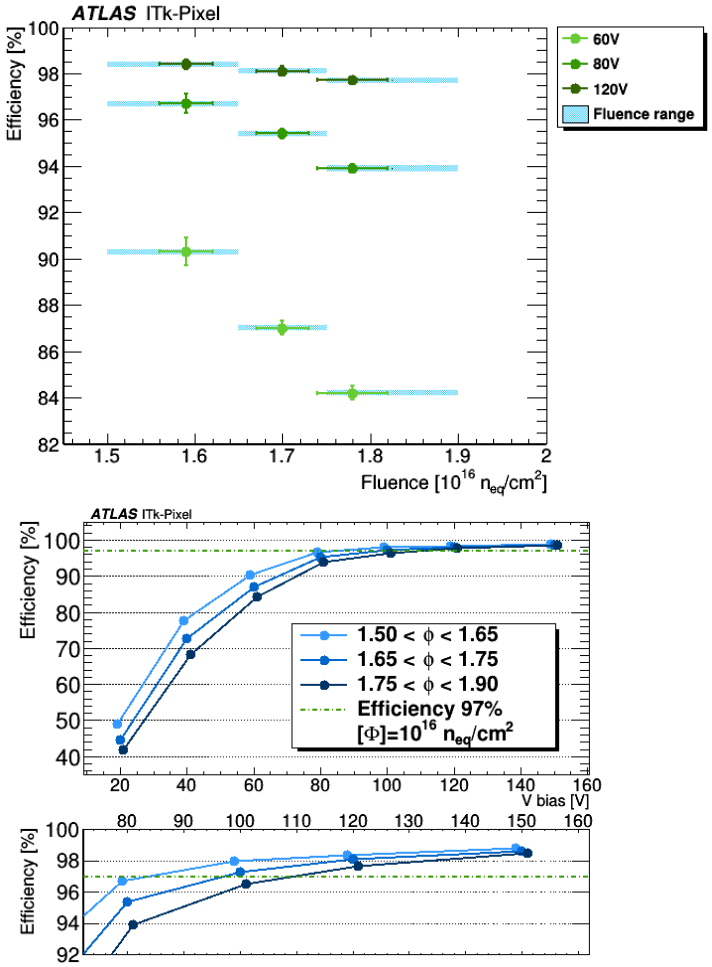

Figure 10: Measured efficiency of SCC3 as a function of fluence for three different values of sensor reverse bias voltage (top) and as a function of reverse bias voltage for the same three fluence ranges in the full bias voltage range considered (middle) and zoomed in the region of the efficiency saturation values (bottom) [25]. In the top plot, the light blue shaded areas represent the arbitrary fluence ranges used to measure each efficiency value, marker's abscissae are the average fluence over that interval, x error bars are the error on the measurement of the fluence integrated at IRRAD (of the order of 5%), the y error bars include the systematic uncertainty on the reconstructed fluence map and the statistical uncertainty on the efficiency measurement over several runs.

~100 V and ~160 V reverse bias is identified by requiring both a high efficiency and a low fraction of failing pixels.

6. Summary and conclusions

The future ATLAS ITk detector will be equipped with 3D sensor modules in the innermost layer (33 mm – 34 mm from the beam axis), where a non ionising fluence up to $1.9 \cdot 10^{16}$ n_{eq}/cm^2 and an ionising dose up to 1 Grad are expected after 2000 fb^{-1} of operation of the HL-LHC. Pre-production 3D modules with 50×50 μm^2 pixel cell sensors produced by FBK and bump-bonded to ITkPixV1.1

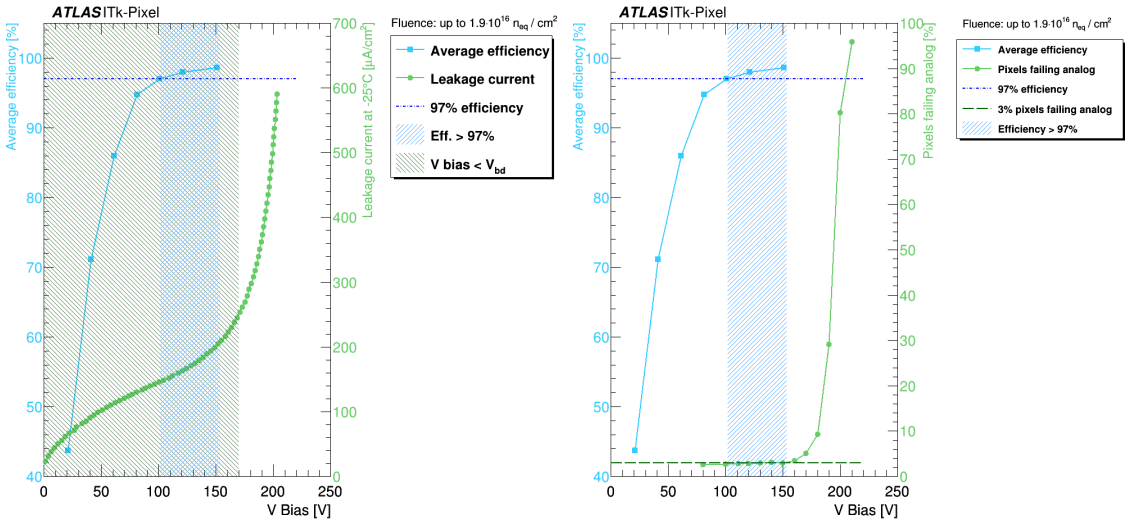

Figure 11: Average efficiency (left scale) and leakage current (right scale) of SCC3 (left) as a function of sensor reverse bias voltage at ultimate integrated fluence (not uniform up to $1.9 \cdot 10^{16} n_{eq}/cm^2$). The solid green area marks the region in which the sensor bias voltage is smaller than the breakdown voltage [25]. Average efficiency (left scale) and fraction of pixels failing the analog scan (right scale) of SCC3 (right) as a function of sensor reverse bias voltage at ultimate integrated fluence [25]. The analog scan is done using the same tuning for all points (target threshold 1000*e* performed at 100 V reverse bias). The dashed green line marks the 3% level of pixels failing the analog scans. In both plots the efficiency is measured with the module perpendicular to the beam over an area with average fluence of $\sim 1.7 \cdot 10^{16}$ n_{eq}/cm^2, the solid blue area marks the region in which the measured efficiency is >97%.

readout chips at IZM have been assembled in Genoa and tested. They have first been tested unirradiated both in the laboratory with X-rays and in test beams (at CERN PS and SPS), showing a hit detection efficiency higher than 97.5% already at 0 V bias and an in-pixel efficiency in the central pixel region >99%. Then they have been irradiated twice, in Bonn and at the CERN IRRAD facility, up to a total integrated not uniform fluence up to $1.9 \cdot 10^{16}$ n_{eq}/cm^2 ($1.5 \cdot 10^{16}$ n_{eq}/cm^2 average) and tested in test beams (at CERN SPS) after each irradiation. The average hit efficiency measured at a fluence of $1 \cdot 10^{16}$ n_{eq}/cm^2 is ~98.5%, higher than the one observed in [9] (~96%) at a similar irradiation value. The average hit efficiency measured on devices irradiated at ultimate fluence is as high as 97% at 80 V, 100 V, 110 V reverse bias applied for an average fluence of $1.59 \cdot 10^{16}$ n_{eq}/cm^2, $1.70 \cdot 10^{16}$ n_{eq}/cm^2, $1.78 \cdot 10^{16}$ n_{eq}/cm^2 respectively. A fraction of pixels failing the analog scan increasing with the applied bias voltage was observed (with tuning performed at 100 V reverse bias used for all voltages applied). The measured performance allows to identify a reasonable operability window (approximately 100 V – 160 V) taking into account the efficiency, the fraction of failing pixels and the breakdown voltage. More devices are planned to be irradiated and tested to confirm the data presented in this report.

Acknowledgments

We gratefully thank the teams of the irradiation facilities at Bonn and IRRAD and the valuable help of people that participated and provided support to the several test beam campaigns.

References

[1] G. Apollinari et al., *High-Luminosity Large Hadron Collider (HL-LHC): Technical Design Report*, CERN Yellow Reports: CERN-2020-010, CERN, Geneva (2020)

[2] ATLAS Collaboration, *The ATLAS Experiment at the CERN Large Hadron Collider*, 2008 JINST **3** S08003

[3] ATLAS Collaboration, *Expected tracking and related performance with the updated ATLAS Inner Tracker layout at the High-Luminosity LHC*, ATL-PHYS-PUB-2021-024

[4] ATLAS collaboration, *ATLAS Inner Tracker Pixel Detector TDR*, Technical Design Report CERN-LHCC-2017-021, CERN, Geneva (2017)

[5] ATLAS collaboration, *ATLAS Inner Tracker Strip Detector TDR*, Technical Design Report CERN-LHCC-2017-005, CERN, Geneva (2017)

[6] J. Bernhard et al., *CERN Proton Synchrotron East Area Facility: Upgrades and renovation during Long Shutdown 2*, CERN-2021-004 (2021)

[7] D. Banerjee et al., *The North Experimental Area at the Cern Super Proton Synchrotron*, CERN-ACC-NOTE-2021-0015 (2021)

[8] M. Boscardin et al., *Advances in 3D sensor technology by using stepper lithography*, Frontiers in Physics - Radiation Detection and Imaging **8**, 625275 (2021)

[9] S. Terzo et al., *Novel 3D Pixel Sensors for the Upgrade of the ATLAS Inner Tracker*, Front. Phys., 21 April 2021, Sec. Radiation Detectors and Imaging (2021)

[10] M. Garcia-Sciveres, F. Loddo, J. Christiansen (RD53 Collaboration), *RD53B Manual*, Tech. Rep. CERN-RD53-PUB-19-002, CERN, Geneva (2019)

[11] J.C. Chistiansen, M.L. Garcia-Sciveres, *RD Collaboration Proposal: Development of pixel readout integrated circuits for extreme rate and radiation*, Tech. Rep. CERN-LHCC-2013-008, LHCC-P-006, CERN, Geneva (2013).

[12] M. Mironova, *Measurements of the radiation damage to the ITkPixV1 chip in X-ray irradiations*, NIM A **1039**, 166947 (2022)

[13] G. Calderini et al., *Test of ITk 3D sensor pre-production modules with ITkPixV1.1 chip*, JINST **18** C01010 (2023)

[14] T. Wittig, *Slim edge studies, design and quality control of planar ATLAS IBL pixel sensors*, PhD Thesis, Dortmund U., DOI: 10.17877/DE290R-5402 (2013)

[15] H. Jansen, S. Spannagel, J. Behr et al., *Performance of the EUDET-type beam telescopes*, EPJ Techn Instrum **3**, 7 (2016).

[16] D. Haas, E. Corrin, M. Poh, *JRA1 - Data acquisition system*, EUDET-Memo-2006-07 (2007)

[17] D. Cussans, *Description of the JRA1 Trigger Logic Unit (TLU), v0.2c*, EUDET-Memo-2009-4 (2009)

[18] T. Heim, *YARR - A PCIe based readout concept for current and future ATLAS Pixel modules*, Proceedings of 22nd International Conference on Computing in High Energy and Nuclear Physics (CHEP2016) 2016, (2017)

[19] P. Ahlburg et al., *EUDAQ - a data acquisition software framework for common beam telescopes*, 2020 JINST **15** P01038

[20] C. Hu et al., *A ten thousand frames per second readout MAPS for the EUDET beam telescope*, CERN-2009-006.47

[21] J. Kröger, S. Spannagel, M. Williams, *User Manual for the Corryvreckan Test Beam Data Reconstruction Framework, Version 1.0*, arXiv:1912.00856 (2019)

[22] S. Ravera, *Development of systems and test of devices for the ATLAS ITk detector moving from R&D to construction*, CERN-THESIS-2022-175

[23] ITk Public Plots, *3D FBK irradiated Pixel modules*, ITK-2022-004

[24] M. Garcia-Sciveres et al., *The RD53A Integrated Circuit*, Technical Report CERN-RD53-PUB-17-001, CERN, Geneva (2017)

[25] ITk Public Plots, *3D FBK irradiated at ultimate fluence*, ITK-2022-005

[26] L. Gaioni (RD53 Collaboration), *Test results and prospects for RD53A, a large scale 65 nm CMOS chip for pixel readout at the HL-LHC*, NIM A **936**, 282-285 (2019)